

# High Methanol Uptake Capacity in Two New Series of Metal–Organic Frameworks: Promising Materials for Adsorption-Driven Heat Pump Applications

Binh T. Nguyen,<sup>†,‡</sup> Ha L. Nguyen,<sup>†</sup> Tranh C. Nguyen,<sup>#</sup> Kyle E. Cordova,<sup>§,⊥</sup> and Hiroyasu Furukawa<sup>\*,§,⊥,||</sup>

<sup>†</sup>Vietnam National University-Ho Chi Minh (VNU-HCM), Ho Chi Minh City 721337, Vietnam

<sup>‡</sup>Department of Chemistry, Ho Chi Minh City Pedagogical University, Ho Chi Minh City 721337, Vietnam

<sup>#</sup>Faculty of Chemistry, University of Science, Vietnam National University-Ho Chi Minh (VNU-HCM), Ho Chi Minh City 721337, Vietnam

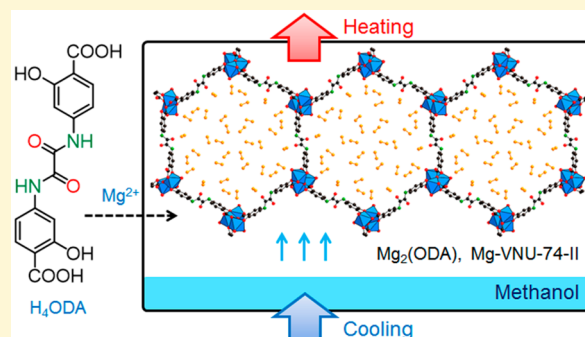
<sup>§</sup>Department of Chemistry and Berkeley Global Science Institute, University of California-Berkeley, Berkeley, California 94720, United States

<sup>⊥</sup>Materials Sciences Division, Lawrence Berkeley National Laboratory, Berkeley, California 94720, United States

<sup>||</sup>Center for Research Excellence in Nanotechnology (CENT), King Fahd University of Petroleum and Minerals, Dhahran 34464, Saudi Arabia

## Supporting Information

**ABSTRACT:** Two new series of metal–organic frameworks (MOFs), termed M-VNU-74-I and -II (where M = Mg, Ni, Co; VNU = Vietnam National University) were designed to expand the methanol uptake capacities with polar amide functionalities. The resulting MOFs, isoreticular to MOF-74, exhibited high porosity (up to 3000 m<sup>2</sup> g<sup>-1</sup>) as well as the highest reported methanol uptake [ $>1$  g g<sup>-1</sup> or  $>400$  cm<sup>3</sup> cm<sup>-3</sup>]. As a representative example, Mg-VNU-74-II was shown to maintain a remarkably high stability and methanol mass transfer capacity for at least 42 ad/desorption cycles (3 days). Indeed, these findings highlight the potential of such materials for practical use in adsorption heat pump applications.



## INTRODUCTION

The U.S. Department of Energy, Building Technologies Office (BTO), has set a 2025 target of reducing residential building primary energy usage by 40% from the 2010 level.<sup>1</sup> Given the fact that primary energy consumption has increased since 2010, meeting such targets through conventional energy conservation (i.e., simply increasing energy efficient processes) is a daunting challenge.<sup>2–5</sup> In fact, an overhaul of current building heating and cooling systems is more likely necessary, in which the establishment and implementation of high coefficient of performance (COP) systems is of top priority.<sup>6–8</sup> To address the BTO's target, emerging technologies have been proposed that exploit thermal batteries for use in air-conditioned buildings. In this process, heating and cooling are driven by the adsorption and evaporation of water, respectively, due to water's high latent heat (40.7 kJ mol<sup>-1</sup>) (Figure 1).<sup>8</sup> However, the low vapor saturation pressure of water (3.17 kPa at 25 °C) presents a conspicuous disadvantage for realizing an effective thermal battery system, as strong interactions between water and the adsorbent are required to achieve high uptake capacities.<sup>8–11</sup>

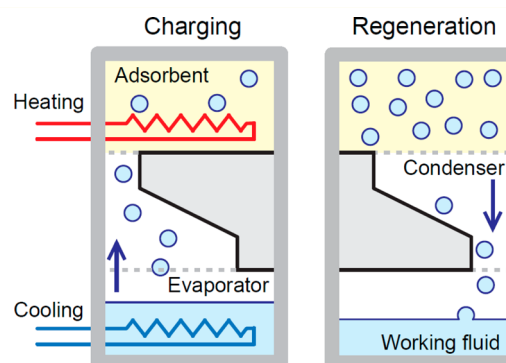


**Figure 1.** Schematic representation of the heating and cooling processes of a thermal battery that are driven by working fluid (e.g., water or methanol) adsorption and evaporation.

Zeolites, a class of crystalline, hydrophilic, microporous aluminosilicates, are well-known to effectively adsorb large

Received: June 16, 2016

Revised: August 1, 2016

amounts of water at relative pressures below 0.05.<sup>12</sup> However, regeneration of these materials requires temperatures as high as 250 °C, which inevitably diminishes the energy efficiency of a zeolite-based thermal battery system.<sup>8</sup> To overcome the challenges presented by water, methanol has been proposed as a potential working fluid due to its higher saturation vapor pressure (17.0 kPa at 25 °C) as well as its relatively high latent heat (34.4 kJ mol<sup>-1</sup>).<sup>8–10,13</sup> Furthermore, methanol has the added benefit of a lower boiling point (64.7 °C), leading to faster adsorption–desorption cycles (due to ease of regeneration).<sup>8–10</sup>

Therefore, it is expected that the overall efficiency of heat release, when utilizing methanol-based thermal batteries, has the potential to outperform its water-based counterparts if suitable adsorbent materials are available.

Metal–organic frameworks (MOFs) are a promising class of crystalline, porous materials for use as adsorbents in thermal battery systems.<sup>9–11</sup> By choosing the appropriate combination of inorganic cluster and organic linkers, the pore structure/environment as well as adsorption enthalpy of a MOF can be easily designed or fine-tuned.<sup>17</sup> Indeed, MOF materials are known to adsorb significant amounts of water and/or methanol vapor, although pressures for condensation of such vapors within the pores remain too high for use in practical applications.<sup>9–11,13,18–35</sup> In this contribution, we describe the development of two new series of MOFs, termed M-VNU-74-I and -II (M = Mg, Ni, Co; VNU = Vietnam National University). Specifically, we report the synthesis and full characterization of six new compounds, M<sub>2</sub>(TDA) [M-VNU-74-I; M = Mg, Ni, or Co, H<sub>4</sub>TDA = 4,4'-(1,4-phenylenebis(carbonylimino))bis(2-hydroxybenzoic acid)], and M<sub>2</sub>(ODA) [M-VNU-74-II; M = Mg, Ni, or Co, H<sub>4</sub>ODA = 4,4'-(oxalylbis(imino))bis(2-hydroxybenzoic acid)]. The MOF design strategy rested on integrating polar amide functionalities within the pore walls in order to increase the storage capacity of methanol working fluid. Based on structural analysis, both M-VNU-74-I and -II are isoreticular (having the same topology), in which the pore metrics were varied by expanding the organic linker used (Figure 2). Indeed, this allowed for a proper evaluation of pore size, framework stability, and functionalization as it relates to methanol adsorption. Methanol isotherm measurements demonstrated that both series exhibited significant methanol uptake, but M-VNU-74-I was found to be structurally unstable under the adsorption conditions. Thus, attention was focused on the M-VNU-74-II series, whose structural stability is stronger and pore diameter is smaller. Accordingly, the highest methanol uptake at appropriately low vapor pressure [ $>0.75 \text{ g g}^{-1}$  ( $>360 \text{ cm}^3 \text{ cm}^{-3}$ ) at  $P/P_0 = 0.27$ ] was observed, and the deliverable amount of methanol, a key parameter for thermal batteries, was also found to be remarkably high (ca.  $250 \text{ cm}^3 \text{ cm}^{-3}$ ). Dynamic adsorption experiments were performed on Mg-VNU-74-II, as a representative example, under varying methanol vapor pressures. These measurements demonstrated that the methanol mass transfer capacity, as a function of temperature and cycle, remained constant over 3 days. Furthermore, the ease of regeneration between each cycle was accomplished under mild conditions (methanol/N<sub>2</sub> flow at 80 °C for 25 min).

## EXPERIMENTAL SECTION

**Materials and General Procedures.** 4-Aminosalicylic acid (99% purity), terephthaloyl chloride ( $\geq 99\%$  purity), magnesium nitrate

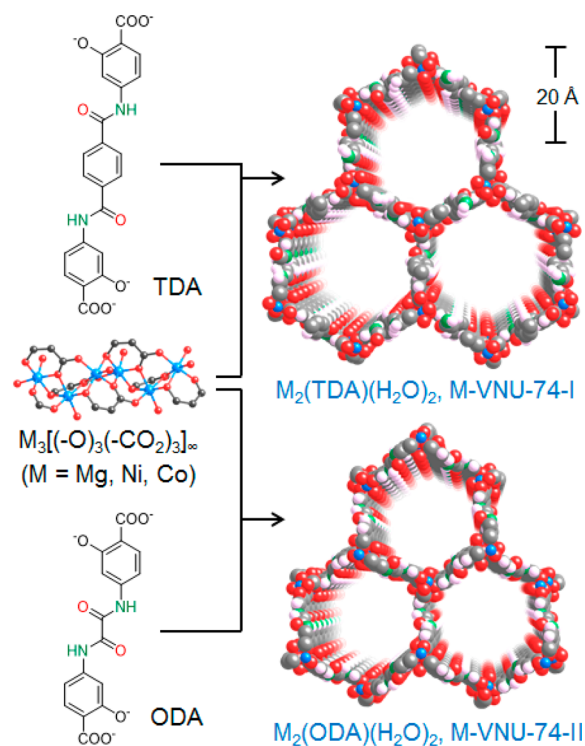


**Figure 2.** Crystal structures of M-VNU-74-I and -II. Similar to MOF-74,<sup>14–17</sup> infinite, rod-shaped metal clusters,  $M_3[(-O)_3(-CO_2)_3]_\infty$  (where M = Mg, Ni, or Co), are joined with either TDA<sup>4-</sup> or ODA<sup>4-</sup> linkers to form M-VNU-74-I and -II, respectively. Atom colors: C, gray; O, red; N, green; H, pink; metal atoms, blue. H atoms of the coordinated water are omitted for clarity.

hexahydrate (99% purity), nickel(II) nitrate hexahydrate, cobalt(II) nitrate hexahydrate ( $\geq 98.0\%$  purity), *N,N*-dimethylformamide (DMF,  $\geq 99\%$  purity), and *N*-methyl-2-pyrrolidone (NMP,  $\geq 99.5\%$  purity) were purchased from Aldrich Chemical Co. Oxalyl chloride (98% purity) was acquired from Acros Organic Co. Anhydrous methanol (99.8% extra dry) and ethanol (EMSURE grade) were purchased from Merck Chemical Co. Finally, diethyl ether ( $>99.5\%$ , extra dry) was obtained from Fisher Scientific. All other chemicals were purchased from commercial vendors and used without further purification, unless otherwise noted.

<sup>1</sup>H and <sup>13</sup>C nuclear magnetic resonance (NMR) spectroscopy measurements were recorded on a Bruker Avance II 500 MHz spectrometer. Chemical shifts are reported in parts per million (ppm) as referenced by tetramethylsilane located at 0 ppm. Coupling constants, *J*, are reported in Hz. Electrospray-ionization mass spectrometry (ESI-MS) was conducted in negative ionization mode on an Agilent 1200 Series high-performance liquid chromatography coupled to a Bruker micrOTOF-Q II mass spectrometer detector. Fourier transform infrared (FT-IR) spectroscopy was measured on a Bruker Vertex 70 spectrometer using potassium bromide (KBr) pellets with output absorption bands described as s, strong; m, medium; w, weak; and br, broad. Elemental microanalyses (EA) were performed on activated or dried samples in the Microanalytical Laboratory of the College of Chemistry at UC Berkeley, using a PerkinElmer 2400 Series II CHNS elemental analyzer (Section S1 in the Supporting Information).

Powder X-ray diffraction (PXRD) data was collected on a Bruker D8 Advance, equipped with a *LyngEye* detector, in reflectance Bragg–Brentano geometry employing Ni filtered (0.2 mm) Cu *K* $\alpha$  radiation (1.54178 Å) at 1600 W (40 kV, 40 mA) power. In a typical PXRD measurement, an activated sample of M-VNU-74-I or -II was spread and leveled on a zero background holder. The  $2\theta$  range was 2–80° with a step size of 0.02° and a fixed counting time of 12.5 s per step for structural refinement (Section S2). Thermogravimetric analysis

(TGA) curves were recorded on a TA Q500 thermal analyzer under air flow (Section S3).

Low-pressure N<sub>2</sub> adsorption experiments were carried out on an Autosorb iQ volumetric gas sorption analyzer. Ultrapure N<sub>2</sub> and He (99.999%) were used for all adsorption measurements. A liquid N<sub>2</sub> bath (77 K) was used in all N<sub>2</sub> isotherm measurements (Section S4). Methanol adsorption measurements were performed on a BEL Japan, Inc. Belsorp-aqua3 using ultrapure He (99.999%) and anhydrous methanol (99.8% extra dry). Manifold temperature was kept at 50 °C to avoid condensation of methanol. Methanol isotherms were measured at 10, 15, and 25 °C for Mg-VNU-74-II and only at 25 °C for the rest of the two series (Section S5). The multicycle methanol isotherm data for Mg-VNU-74-II was collected in one measurement, in which the sample was automatically evacuated at 25 °C for 3 h between each cycle.

**Synthesis of Linkers, H<sub>4</sub>TDA and H<sub>4</sub>ODA.** In general, H<sub>4</sub>TDA and H<sub>4</sub>ODA linkers were synthesized from *N*-acylation reactions of 4-aminosalicylic acid with terephthaloyl chloride and oxalyl chloride, respectively. Full synthetic details can be found in Section S1.

**M-VNU-74-I and -II Synthesis.** In general, both M-VNU-74-I and -II were synthesized through solvothermal reactions between H<sub>4</sub>TDA or H<sub>4</sub>ODA linker and the appropriate M<sup>2+</sup> cation (M<sup>2+</sup> = Mg, Ni, or Co), respectively, in a DMF, ethanol, and water (15/1/1, v/v) solvent system. For full synthetic details for all members of both series, please refer to Section S1.

**Synthesis and Activation of Mg-VNU-74-I.** Mg(NO<sub>3</sub>)<sub>2</sub>·6H<sub>2</sub>O (31.8 mg, 0.124 mmol) and H<sub>4</sub>TDA (18.5 mg, 0.0424 mmol) were dissolved in a 10 mL glass vial containing 3.75 mL of DMF. The vial was sealed and sonicated for 30 min until the solid was completely dissolved. To this solution, 0.25 mL of ethanol and 0.25 mL of deionized water were added. The resulting solution was heated at 120 °C for 2 d in an isothermal oven, after which time colorless, needle-shaped crystals were obtained (58% yield based on the organic linker). The as-synthesized Mg-VNU-74-I was subsequently washed with DMF (6 × 5 mL) over 2 d before solvent exchanging with dry MeOH (4 × 5 mL, each d for 3 d). The MeOH exchanged samples were activated by the supercritical CO<sub>2</sub> method using a Tousimis Samdri-PVT-3D critical point dryer.<sup>16,19</sup> The resulting samples were further activated under reduced pressure (20 mTorr) at room temperature for 24 h, followed by evacuation at 70 °C for 12 h. All subsequent analyses were performed using activated samples. FT-IR (KBr, 4000–400 cm<sup>-1</sup>): 3195 (br), 2748 (w), 1602 (m), 1566 (s), 1541 (w), 1483 (w), 1423 (s), 1373 (s), 1294 (s), 1245 (s), 1190 (w), 1157 (w), 1112 (w), 1014 (w), 981 (w), 846 (w), 783 (m), 763 (m), 705 (m), 680 (m), 648 (m), 632 (w), 609 (s). EA (activated sample): Calcd for Mg<sub>2</sub>(C<sub>22</sub>H<sub>12</sub>N<sub>2</sub>O<sub>8</sub>)·3H<sub>2</sub>O: C, 49.36; H, 3.40; N, 5.24%. Found: C, 49.28; H, 3.68; N, 5.10%.

**Synthesis and Activation of Mg-VNU-74-II.** Mg(NO<sub>3</sub>)<sub>2</sub>·6H<sub>2</sub>O (43.5 mg, 0.170 mmol) and H<sub>4</sub>ODA (15.3 mg, 0.0425 mmol) were dissolved in a 10 mL glass vial containing 3.75 mL of DMF. The vial was sealed and sonicated for 20 min and then heated lightly until the solid was completely dissolved. To this solution, 0.25 mL of ethanol and 0.25 mL of deionized water were added. The resulting solution was heated at 120 °C for 2 d in an isothermal oven, after which time colorless needle-shaped crystals were obtained (65% yield based on the organic linker). The activation procedure was similar to that reported for Mg-VNU-74-II (Section S3). FT-IR (KBr, 4000–400 cm<sup>-1</sup>): 3294 (br), 2929 (w), 1672 (w), 1600 (s), 1568 (s), 1500 (m), 1477 (m), 1415 (s), 1375 (s), 1280 (w), 1245 (m), 1159 (w), 1099 (w), 993 (w), 977 (w), 825 (w), 777 (m), 734 (s), 678 (s), 626 (s), 603 (s). EA (activated sample): Calcd for Mg<sub>2</sub>(C<sub>16</sub>H<sub>8</sub>N<sub>2</sub>O<sub>8</sub>)·2.6H<sub>2</sub>O: C, 42.52; H, 2.95; N, 6.20%. Found: C, 42.56; H, 3.46; N, 5.77%.

**Structural Modeling and Elucidation.** A structural model of M-VNU-74-I or -II was executed by using the *Materials Visualizer* module of *Materials Studio* software (*Materials Studio* v. 5.5.0.0, 2010, Accelrys Software Inc.). As a representative example, Mg-VNU-74-II is used to describe the modeling method that was employed for all members of both series. Due to the connectivity of the TDA and ODA linkers, the crystal structures of M-VNU-74-I and -II are expected to be isorectangular to each other and to the well-known M-MOF-74.<sup>14–17</sup>

Thus, both structural modeling and refinement of Mg-VNU-74-II were carried out based on the single crystal structure of Zn-MOF-74.<sup>14</sup> Accordingly, the organic linker, ODA, was constructed in the *GaussView* graphical interface for *Gaussian* in order to identify suitable resonance geometries. Next, this optimized ODA was connected to the infinite-rod shaped Mg metal cluster that is characteristic of M-MOF-74 structures. There were no guest molecules incorporated into the pores of the model, which leads to the assumption of an empty framework. Upon completion of this structural model, an energetic minimization was performed by the universal force field carried out in the *Forcite* module of *Materials Studio*. The unit cell parameters were also optimized until proper convergence was achieved (energy convergence criteria were set at 10<sup>-4</sup> kcal mol<sup>-1</sup>). A similar procedure was carried out for TDA-containing structures.

**Methanol Transference Cycling Experiment.** The Q500 TGA was coupled with an HG-100 vapor generator from L&C Science Technology Co. The TGA chamber was continuously flushed with dry N<sub>2</sub> (10 mL min<sup>-1</sup>) as the balance flow and MeOH/N<sub>2</sub> mixture as the sample flow (90 mL min<sup>-1</sup>). In each experiment, the methanol pressure was set at 4.3, 8.5, 11.9, 15.3, and 16.9 kPa to build relative methanol humidity of 22, 45, 63, 81, and 89%, respectively, at 25 °C. Roughly 15 mg of activated material was loaded for each experiment. For the adsorption step, the furnace temperature was kept at 25 °C for 50 min under the methanol-containing N<sub>2</sub> flow. Next, the temperature was increased to 80 °C (5 °C min<sup>-1</sup>), where it was kept constant for 15 min under methanol/N<sub>2</sub> flow. The furnace temperature was naturally cooled down to 25 °C to start the next adsorption cycle. There was no observed methanol condensation in the system as confirmed by a blank, control measurement (Section S6). The sample mass was not corrected for the buoyancy effect, which may lead to a slight underestimation of the methanol mass transfer capacity.

## RESULTS AND DISCUSSION

In order to maximize the adsorption capacities of methanol working fluid in the pores of a MOF structure, we designed two linkers of differing sizes that incorporated moderately polar amide groups within its backbone. The pore expansion with polar functionalities is a rational strategy, since the interactions between the working pair (i.e., MOF and methanol) generally decreases by pore expansion, leading to a reduction in the volumetric storage capacity.

The synthetic procedures for realizing the M-VNU-74-I and -II series were developed, with slight modifications, based on the conditions used for MOF-74 (Section S1).<sup>16</sup> Microcrystalline powders, obtained in 60–75% yield, were achieved for all members of the M-VNU-74-I and -II series. Prior to structural analysis, both series were solvent exchanged and subsequently activated to remove occluded guest species. Structural elucidation was carried out via PXRD analysis, in which the experimental patterns were compared with the calculated patterns generated from structural models (Figure 3, Section S2). Full pattern profile fitting (unit cell information) and Pawley refinement was then performed, resulting in convergence with satisfactory residual values (e.g.,  $R_{wp} = 4.46\%$ ,  $R_p = 3.41\%$ , and  $R_{wp} = 6.02\%$ ,  $R_p = 4.58\%$  for Mg-VNU-74-I and Mg-VNU-74-II, respectively). M-VNU-74-I and -II are, in fact, isorectangular to MOF-74. The structures of both series contain infinite, rod-shaped secondary building units that are linked together by either TDA<sup>4-</sup> or ODA<sup>4-</sup> linkers (Figure 2). This results in an *etb* topology composed of octahedrally coordinated divalent metal atoms highlighted by the formation of one-dimensional, hexagonal channels that are lined with amide groups from the linkers. From the crystal structures, the pore apertures (size of diagonal dimension) were calculated to be 26.4/22.5, 27.3/23.6, and 27.4/23.2 Å for Mg-VNU-74-I/-II, Ni-VNU-74-I/-II, and Co-VNU-74-I/-II, respectively (Table

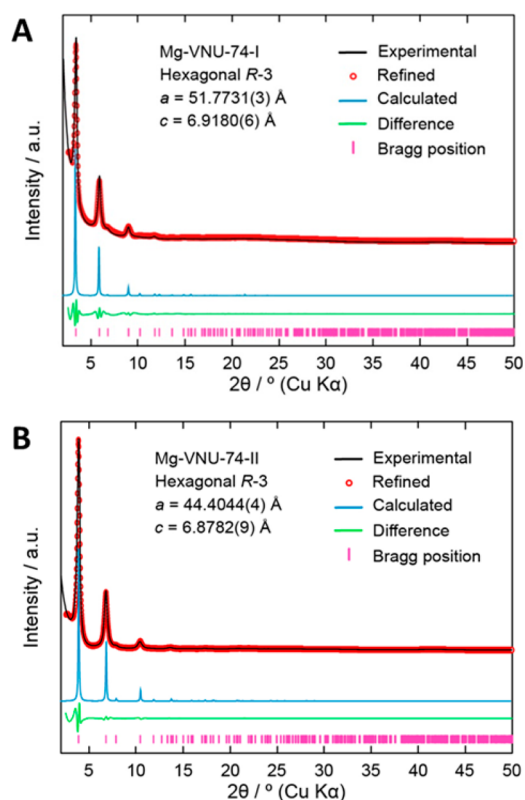


**Figure 3.** PXRD analysis of activated Mg-VNU-74-I (A) and -II (B). The experimental pattern (blue), refined pattern (red circles), and calculated pattern (black). The difference plot (green) and Bragg positions (pink) are provided for comparison.

1). For comparison, the pore apertures of M-VNU-74-I and -II are slightly larger than and similar to those of IRMOF-74-II (19.5 Å) and -III (27.3 Å), respectively.<sup>16</sup>

TGA measurements demonstrated that all members were thermally robust with decomposition occurring at temperatures >300 °C (Section S3). In order to examine the porosity, N<sub>2</sub> isotherms at 77 K were measured, and the corresponding profiles were classified as Type IV, indicative of mesoporous materials (Figure 4). Using the saturation uptake ( $P/P_0 = 0.9$ ), the calculated pore volumes were 0.84/1.08, 1.10/1.27, and

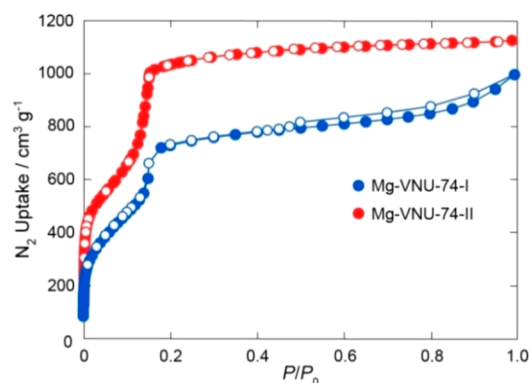


**Figure 4.** N<sub>2</sub> adsorption isotherms at 77 K for Mg-VNU-74-I (blue) and Mg-VNU-74-II (red). Closed and open circles represent the adsorption and desorption branches, respectively. The connecting line is provided as a guide.

1.42/1.68 cm<sup>3</sup> g<sup>-1</sup> for Ni-VNU-74-I/-II, Co-VNU-74-I/-II, and Mg-VNU-74-I/-II, respectively (Table 1). Furthermore, high porosity of both series was demonstrated by their calculated Brunauer–Emmett–Teller (BET) surface areas (ranging from 1820 to 3030 m<sup>2</sup> g<sup>-1</sup> for Ni-VNU-74-I and Mg-VNU-74-II, respectively, Table 1). We note that the surface area of Mg-VNU-74-II (>3000 m<sup>2</sup> g<sup>-1</sup>) is one of the highest values reported for isoreticular MOF-74 structure [3270 m<sup>2</sup> g<sup>-1</sup> for Mg<sub>2</sub>(dobdc), dobpdcc = 4,4'-dioxido-3,3'-biphenyldicarboxylate].<sup>14–16</sup>

Methanol adsorption isotherms at 25 °C were subsequently measured for the amide-containing M-VNU-74-I and -II series. Accordingly, the isotherms for the M-VNU-74-I series displayed convoluted profiles, which was attributed to structural collapse upon remeasuring N<sub>2</sub> isotherms at 77 K after the methanol adsorption measurements were completed (Section S5). For the M-VNU-74-II series, fully reversible, Type-IV methanol isotherms were observed (Figure 3). At  $P/P_0 < 0.05$ , the isotherms exhibit steep uptake, followed by a second, steep uptake step (pore is filled) at  $P/P_0 = 0.2–0.3$ . Interestingly, there was negligible hysteresis detected for all members of this series, which, in general, points to a lower required regeneration energy needed for subsequent reuse.<sup>10</sup> Furthermore, the maximum methanol capacity ( $P/P_0 = 0.7$ ) of the M-VNU-74-II series was remarkably high; notably, 1.04, 0.90, and 0.75 g g<sup>-1</sup>

**Table 1.** Structural and Methanol Adsorption Properties for the M-VNU-74-I and -II Series in Comparison with Similarly Related High-Performing MOFs

| material                    | $A_{\text{BET}}$ (m <sup>2</sup> g <sup>-1</sup> ) <sup>a</sup> | crystal density (g cm <sup>-3</sup> ) <sup>b</sup> | pore diameter (Å) <sup>c</sup> | pore volume (cm <sup>3</sup> g <sup>-1</sup> ) <sup>d</sup> | maximum capacity ( $q_{\text{max}}$ ; g g <sup>-1</sup> ) <sup>e</sup> | maximum capacity ( $q_{\text{max}}$ ; cm <sup>3</sup> cm <sup>-3</sup> ) <sup>e</sup> | deliverable amount (cm <sup>3</sup> cm <sup>-3</sup> ) <sup>f</sup> |
|-----------------------------|-----------------------------------------------------------------|----------------------------------------------------|--------------------------------|-------------------------------------------------------------|------------------------------------------------------------------------|---------------------------------------------------------------------------------------|---------------------------------------------------------------------|
| Mg-VNU-74-I                 | 2410                                                            | 0.48                                               | 26.4                           | 1.42                                                        | 0.46                                                                   | 155                                                                                   | 48                                                                  |
| Ni-VNU-74-I                 | 1820                                                            | 0.59                                               | 27.3                           | 0.84                                                        | 0.77                                                                   | 316                                                                                   | 87                                                                  |
| Co-VNU-74-I                 | 2110                                                            | 0.57                                               | 27.6                           | 1.10                                                        | 0.65                                                                   | 257                                                                                   | 82                                                                  |
| Mg-VNU-74-II                | 3030                                                            | 0.56                                               | 22.5                           | 1.68                                                        | 1.04                                                                   | 407                                                                                   | 243                                                                 |
| Ni-VNU-74-II                | 2180                                                            | 0.70                                               | 23.6                           | 1.08                                                        | 0.75                                                                   | 367                                                                                   | 196                                                                 |
| Co-VNU-74-II                | 2480                                                            | 0.69                                               | 23.2                           | 1.27                                                        | 0.90                                                                   | 435                                                                                   | 256                                                                 |
| MIL-101(Cr) <sup>6,36</sup> | 4230                                                            | 0.48                                               | 29, 34                         | 1.40                                                        | 1.15                                                                   | 386                                                                                   | 151                                                                 |
| MIL-100(Cr) <sup>6,37</sup> | 1900                                                            | 0.71                                               | 25, 29                         | 0.85                                                        | 0.67                                                                   | 333                                                                                   | 159                                                                 |
| UiO-67 <sup>6,38</sup>      | 2500                                                            | 0.71                                               | 12, 23                         | 0.93                                                        | 0.34                                                                   | 169                                                                                   | 208                                                                 |
| ZIF-8 <sup>6,39</sup>       | 1580                                                            | 0.92                                               | 11.6                           | 0.48                                                        | 0.37                                                                   | 238                                                                                   | 187                                                                 |

<sup>a</sup>Calculated by the BET method. <sup>b</sup>Based on refined crystal structures. <sup>c</sup>Diagonal dimension. <sup>d</sup>Determined from the N<sub>2</sub> isotherm at 77 K. <sup>e</sup>MeOH capacity at saturation, 298 K. <sup>f</sup>Calculated by subtracting the uptake at the operational desorption relative pressure ( $P/P_0 = 0.1$ ) from the maximum uptake at the operational adsorption relative pressure ( $P/P_0 = 0.3$ ).

(407, 435, and 367  $\text{cm}^3 \text{cm}^{-3}$ ) for Mg-VNU-74-II, Co-VNU-74-II, and Ni-VNU-74-II, respectively (Figure 5). These

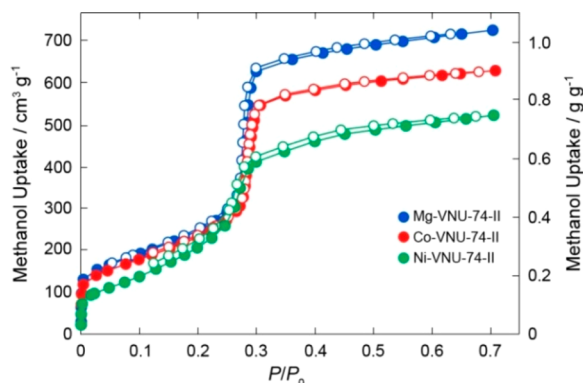


**Figure 5.** Methanol adsorption isotherms at 25 °C for Mg- (blue), Co- (red), and Ni-VNU-74-II (green). Closed and open circles represent the adsorption and desorption branches, respectively. The connecting line is provided as a guide.

maximum capacity values are among the highest reported for MOFs.<sup>9,10,13</sup> We note that an important consideration for assessing adsorbent materials for methanol-based thermal batteries is the deliverable amount of methanol of the material at relevant operating pressures ( $P/P_0 = 0.1\text{--}0.3$  is typically proposed).<sup>40</sup> Although MIL-101(Cr) has a high maximum gravimetric uptake capacity, the methanol isotherm profile demonstrates a smaller deliverable amount of methanol than Mg-VNU-74-II [0.45 and 0.62  $\text{g g}^{-1}$  (151 and 243  $\text{cm}^3 \text{cm}^{-3}$ ) at  $P/P_0 = 0.1\text{--}0.3$  for MIL-101(Cr) and Mg-VNU-74-II, respectively]. This finding suggests that the methanol usability of Mg-VNU-74-II is higher than MIL-101(Cr) in both gravimetric and volumetric units. The coverage-dependent isosteric enthalpy of adsorption ( $Q_{st}$ ) was then calculated for the M-VNU-74-II series by fitting the respective methanol adsorption isotherms at 10, 15, and 25 °C (Section S5). The resulting isotherms all display the same Type-IV profile, in which the maximum capacities were found to vary little with temperature. This implies that MeOH molecules easily condense within the respective MOF pores. Using the Clausius–Clapeyron equation, the average  $Q_{st}$  values, calculated at the middle part of the slope, for Mg-, Ni-, and Co-VNU-74-II were 44.6, 44.6, and 46.4  $\text{kJ mol}^{-1}$ , respectively. The  $Q_{st}$  values are comparable with other reported methanol adsorbents and far higher than the latent heat of methanol (34.4  $\text{kJ mol}^{-1}$ ).<sup>8</sup> These findings, in conjunction with the remarkably high deliverable amount of methanol at relevant operating pressures, strongly points to the M-VNU-74-II series possessing high heat transfer capacities as well—an important characteristic necessary for methanol-based thermal batteries.

In order to be applied toward cooling (air-conditioning) processes [temperatures of the evaporator ( $T_{ev}$ ) and condenser ( $T_{con}$ ) are set at 283 and 303 K, respectively], the volumetric working capacity ( $\Delta W$ ) and COP of M-VNU-74-II were determined as a function of desorption temperature ( $T_d$ ) (Figure S28, Section S5).<sup>10,13</sup> Accordingly, high volumetric working capacities of 0.41, 0.33, and 0.45  $\text{cm}^3 \text{cm}^{-3}$  for Mg-VNU-74-II, Ni-VNU-74-II, and Co-VNU-74-II, respectively, were reached at a low desorption temperature ( $T_d < 355$  K). These  $\Delta W$  values are competitive with the commercially available activated carbon/methanol working pair (G32-H)

whereas the  $\text{COP}_C$  values of 0.82, 0.80, and 0.79 for the Mg-VNU-74-II, Ni-VNU-74-II, and Co-VNU-74-II/methanol working pair, respectively (Figure S28, Section S5), are higher than G32-H/methanol (0.60) as well as benchmark adsorbent/water working pairs (0.70 for both AQSOA-Z01 and -Z02) at the same desorption temperature of 80 °C.<sup>13</sup>

On the basis of its high porosity and methanol adsorption properties, Mg-VNU-74-II was chosen as a representative example for demonstrating the applicability of such materials for use in thermal battery systems. Accordingly, a multicycle, continuous methanol isotherm at 25 °C (9 cycles) was measured for Mg-VNU-74-II in order to investigate its stability for long-term use (Section S5). After the first cycle, the total uptake slightly decreased from 1.04 to 0.91  $\text{g g}^{-1}$ ; however, the deliverable amount of methanol remained the same [0.62  $\text{g g}^{-1}$  (243  $\text{cm}^3 \text{cm}^{-3}$ ),  $P/P_0 = 0.1\text{--}0.3$ ]. These values remained constant until the end of the cycling measurement with the Type-IV profile being fully retained and no hysteresis appearing during the desorption processes. Upon conclusion of the multicycle isotherm, a  $\text{N}_2$  isotherm at 77 K measurement demonstrated that the porosity of Mg-VNU-74-II was preserved.

Dynamic adsorption measurements, in which the methanol mass transfer capacity of Mg-VNU-74-II was measured in situ under a specific constant methanol vapor, were then carried out (Section S6).<sup>29–35</sup> These measurements were performed at various relative methanol humidities (from 22% to 89%) at 25 °C. Accordingly, for each condition, the transferred weight of methanol was continuously recorded over 42 adsorption/desorption cycles, which lasted 3 d. The amount of transferred methanol mass remained relatively constant over these cycles with resulting average values of 0.11, 0.52, 0.60, 0.61, and 0.62  $\text{g g}^{-1}$  for 22, 45, 63, 81, and 89% of methanol saturation pressure, respectively (Figure 6 and Section S6). These values are slightly

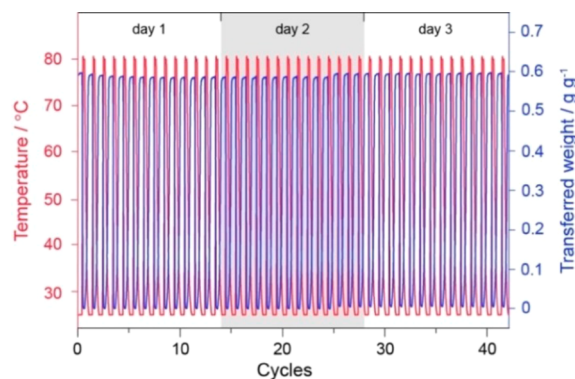


**Figure 6.** Methanol mass transfer capacity within Mg-VNU-74-II as a function of temperature at constant relative methanol humidity (63%). Prior to measuring, Mg-VNU-74-II was exposed to relative methanol humidity for  $\sim 50$  min to equilibrate. The initial point was then set and the cycling measurements were initiated. The minimum value of the sample weight during the measurement was set to 0  $\text{g g}^{-1}$ .

lower than the methanol uptake (i.e., isotherm data) after the second cycle (ca. 0.85  $\text{g g}^{-1}$  in higher methanol vapor pressure region, Figure S29, Section S5), because the relative methanol humidity during the regeneration (80 °C of the furnace temperature) is 4–8%. This indicates that more than 0.1  $\text{g g}^{-1}$  of methanol can remain in the pores even after a prolonged regeneration process under the present experimental conditions.

It is interesting to note that mass transfer essentially reached its maximum value at 63% of relative methanol humidity in a short adsorption time ( $\sim 75$  min) (Figure 6). The process time for each cycle took  $\sim 100$  min to complete, which is considerably faster than previously reported MOF/water working pairs (200–300 min).<sup>29–35</sup> In terms of regeneration between each cycle, Mg-VNU-74-II was recovered by simply heating the sample at 80 °C for 25 min without the need for any evacuation. This is in contrast to reported MOF/water systems, in which a high temperature (140 °C) and evacuation is often required.<sup>29–35</sup> Finally, the structural robustness of Mg-VNU-74-II after completion of the dynamic cycling experiments was proven by performing PXRD and N<sub>2</sub> isotherm measurements at 77 K (Section S6).

The feasibility of applying Mg-VNU-74-II to practical working conditions was assessed by preparing pelletized samples using a conventional press under various pressures [1000, 2000, 5000, and 10000 psi (68, 136, 340, and 680 atm)].<sup>41</sup> The crystallinity and the porosity of the pelletized Mg-VNU-74-II decreased when the magnitude of the pressure increased (Section S5). However, the sample pelletized at 2000 psi (136 atm) exhibited only a 20% decrease in N<sub>2</sub> uptake capacity and a slight decrease in the deliverable amount of methanol from 0.62 to 0.47 g g<sup>-1</sup> in comparison to the pristine, microcrystalline powder sample of Mg-VNU-74-II (Figure 7).

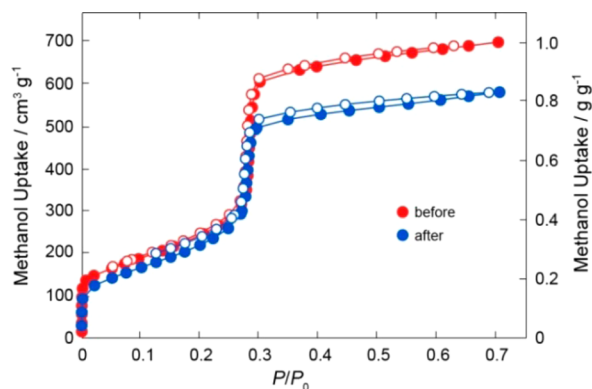


**Figure 7.** Methanol adsorption isotherm at 25 °C of Mg-VNU-74-II before and after pelletizing at 2000 psi (136 atm). Closed and open circles represent the adsorption and desorption branches, respectively. The connecting line is provided as a guide.

## CONCLUSIONS

In conclusion, the synthesis and full characterization of two new isoreticular series of MOFs, termed M-VNU-74-I and -II (where M = Mg, Ni, or Co), are reported. Both series were proven to be highly porous with Mg-VNU-74-II exhibiting one of the highest surface areas ( $>3000$  m<sup>2</sup> g<sup>-1</sup>) of any reported isoreticular M-MOF-74 structure. Due to the high porosity and large pore volume, the M-VNU-74-II series demonstrated the highest reported methanol uptake capacity ( $>400$  cm<sup>3</sup> cm<sup>-3</sup> for Mg- and Co-VNU-74-II) and deliverable amount (ca. 250 cm<sup>3</sup> cm<sup>-3</sup> for Mg- and Co-VNU-74-II) at relevant operating conditions with respect to thermal battery systems. As a representative example, dynamic adsorption experiments were performed on Mg-VNU-74-II, which detailed the methanol mass transfer capacity (varying relative methanol humidities) as a function of temperature, and cycles remained constant over at least 3 days. Furthermore, the shortest cycling time (100 min)

for any reported MOF material was observed. These findings highlight a strategy moving forward for realizing the potential of such materials for use in thermal battery systems.

## ASSOCIATED CONTENT

### Supporting Information

The Supporting Information is available free of charge on the ACS Publications website at DOI: 10.1021/acs.chemmater.6b02431.

Synthesis and full characterization specifics, powder X-ray diffraction data, and N<sub>2</sub> and methanol adsorption experiments and analyses (PDF)

## AUTHOR INFORMATION

### Corresponding Author

\* (H. Furukawa) E-mail: furukawa@berkeley.edu.

### Funding

This work was supported by VNU-HCM (A2015-50-01-HĐ-KHCN) and the United States Office of Naval Research Global: Naval International Cooperative Opportunities in Science and Technology Program (No. N62909-15-1N056).

### Notes

The authors declare no competing financial interest.

## ACKNOWLEDGMENTS

We acknowledge the Center for Innovative Materials and Architectures for facility use and equipment and thank Prof. Omar M. Yaghi (UC Berkeley) for his support. Finally, we are grateful to Ms. Tien N. H. Lo (VNU-HCM) for her preliminary work on this project.

## REFERENCES

- (1) Refer to the United States Department of Energy (DOE), Building Technologies Office website: <http://energy.gov/eere/buildings/residential-buildings-integration> (accessed on June 16, 2016).
- (2) Dixon, R. K.; McGowan, E.; Onysko, G.; Scheer, R. M. US Energy Conservation and Efficiency Policies: Challenges and Opportunities. *Energy Policy* **2010**, *38*, 6398–6408.
- (3) Lewis, N. S.; Nocera, D. G. Powering the Planet: Chemical Challenges in Solar Energy Utilization. *Proc. Natl. Acad. Sci. U. S. A.* **2006**, *103*, 15729–15735.
- (4) Yang, L.; Yan, H.; Lam, J. C. Thermal Comfort and Building Energy Consumption Implications—A review. *Appl. Energy* **2014**, *115*, 164–173.
- (5) Pérez-Lombard, L.; Ortiz, J.; Pout, C. A Review on Buildings Energy Consumption Information. *Energy Build.* **2008**, *40*, 394–398.
- (6) (a) Srivastava, N. C.; Eames, I. W. A review of Adsorbents and Adsorbates in Solid-Vapour Adsorption Heat Pump Systems. *Appl. Therm. Eng.* **1998**, *18*, 707–714.
- (7) Meunier, F. Solid Sorption: An Alternative to CFCs. *Heat Recovery Syst. CHP* **1993**, *13*, 289–295.
- (8) Wang, L. W.; Wang, R. Z.; Oliveira, R. G. A Review on Adsorption Working Pairs for Refrigeration. *Renewable Sustainable Energy Rev.* **2009**, *13*, 518–534.
- (9) Jeremias, F.; Fröhlich, D.; Janiak, C.; Henninger, S. K. Water and Methanol Adsorption on MOFs for Cycling Heat Transformation Processes. *New J. Chem.* **2014**, *38*, 1846–1852.
- (10) de Lange, M. F.; van Velzen, B. L.; Ottevanger, C. P.; Verouden, K. J. F. M.; Lin, L.; Vlugt, T. J. H.; Gascon, J.; Kapteijn, F. Metal–Organic Frameworks in Adsorption-Driven Heat Pumps: The Potential of Alcohols as Working Fluids. *Langmuir* **2015**, *31*, 12783–12796.

- (11) Burtch, N. C.; Jasuja, H.; Walton, K. S. Water Stability and Adsorption in Metal-Organic Frameworks. *Chem. Rev.* **2014**, *114*, 10575–10612.
- (12) Henninger, S. K.; Schmidt, F. P.; Henning, H.-M. Water Adsorption Characteristics of Novel Materials for Heat Transformation Applications. *Appl. Therm. Eng.* **2010**, *30*, 1692–1702.
- (13) de Lange, M. F.; Verouden, K. J. F. M.; Vlugt, T. J. H.; Gascon, J.; Kapteijn, F. Adsorption-Driven Heat Pumps: The Potential of Metal-Organic Frameworks. *Chem. Rev.* **2015**, *115*, 12205–12250.
- (14) Rosi, N. L.; Kim, J.; Eddaoudi, M.; Chen, B.; O’Keeffe, M.; Yaghi, O. M. Rod Packings and Metal-Organic Frameworks Constructed from Rod-Shaped Secondary Building Units. *J. Am. Chem. Soc.* **2005**, *127*, 1504–1518.
- (15) McDonald, T. M.; Lee, W. R.; Mason, J. A.; Wiers, B. M.; Hong, C. S.; Long, J. R. Capture of Carbon Dioxide from Air and Flue Gas in the Alkylamine-Appended Metal-Organic Framework  $m\text{-mmen-Mg}_2(\text{dobpdc})$ . *J. Am. Chem. Soc.* **2012**, *134*, 7056–7065.
- (16) Deng, H.; Grunder, S.; Cordova, K. E.; Valente, C.; Furukawa, H.; Hmadeh, M.; Gándara, F.; Whalley, A. C.; Liu, Z.; Asahina, S.; Kazumori, H.; O’Keeffe, M.; Terasaki, O.; Stoddart, J. F.; Yaghi, O. M. Large-Pore Apertures in a Series of Metal-Organic Frameworks. *Science* **2012**, *336*, 1018–1023.
- (17) Furukawa, H.; Cordova, K. E.; O’Keeffe, M.; Yaghi, O. M. The Chemistry and Applications of Metal-Organic Frameworks. *Science* **2013**, *341*, 1230444.
- (18) Canivet, J.; Fateeva, A.; Guo, Y.; Coasne, B.; Farrusseng, D. Water Adsorption in MOFs: Fundamentals and Applications. *Chem. Soc. Rev.* **2014**, *43*, 5594–5617.
- (19) Furukawa, H.; Gándara, F.; Zhang, Y. B.; Jiang, J.; Queen, W. L.; Hudson, M. R.; Yaghi, O. M. Water Adsorption in Porous Metal-Organic Frameworks and Related Materials. *J. Am. Chem. Soc.* **2014**, *136*, 4369–4381.
- (20) Ko, N.; Choi, P. G.; Hong, J.; Yeo, M.; Sung, S.; Cordova, K. E.; Park, H. J.; Yang, J. K.; Kim, J. Tailoring The Water Adsorption Properties of MIL-101 Metal-Organic Frameworks by Partial Functionalization. *J. Mater. Chem. A* **2015**, *3*, 2057–2064.
- (21) Ehrenmann, J.; Henninger, S. K.; Janiak, C. Water Adsorption Characteristics of MIL-101 for Heat-Transformation Applications of MOFs. *Eur. J. Inorg. Chem.* **2011**, *2011* (4), 471–474.
- (22) Cmarik, G. E.; Kim, M.; Cohen, S. M.; Walton, K. S. Tuning the Adsorption Properties of UiO-66 via Ligand Functionalization. *Langmuir* **2012**, *28*, 15606–15613.
- (23) Akiyama, G.; Matsuda, R.; Sato, H.; Hori, A.; Takata, M.; Kitagawa, S. Effect of functional groups in MIL-101 on water sorption behavior. *Microporous Mesoporous Mater.* **2012**, *157*, 89–93.
- (24) Wade, C. R.; Corrales-Sanchez, T. C.; Narayan, T. C.; Dincă, M. Postsynthetic Tuning of Hydrophilicity in Pyrazolate MOFs to Modulate Water Adsorption Properties. *Energy Environ. Sci.* **2013**, *6*, 2172–2177.
- (25) Biswas, S.; Ahnfeldt, T.; Stock, N. New Functionalized Flexible Al-MIL-53-X (X = -Cl, -Br, -CH<sub>3</sub>, -NO<sub>2</sub>, -(OH)<sub>2</sub>) Solids: Syntheses, Characterization, Sorption, and Breathing Behavior. *Inorg. Chem.* **2011**, *50*, 9518–9526.
- (26) Ko, N.; Sung, S.; Cordova, K. E.; Park, H. J.; Yang, J. K.; Kim, J.; Hong, J. A Significant Enhancement of Water Vapour Uptake at Low Pressure by Amine-Functionalization of UiO-67. *Dalton Trans.* **2015**, *44*, 2047–2051.
- (27) Küsgens, P.; Rose, M.; Senkovska, I.; Fröde, H.; Henschel, A.; Siegle, S.; Kaskel, S. Characterization of Metal-Organic Frameworks by Water Adsorption. *Microporous Mesoporous Mater.* **2009**, *120*, 325–330.
- (28) Taylor, J. M.; Vaidhyanathan, R.; Iremonger, S. S.; Shimizu, G. K. H. Enhancing Water Stability of Metal-Organic Frameworks via Phosphonate Monoester Linkers. *J. Am. Chem. Soc.* **2012**, *134*, 14338–14340.
- (29) Henninger, S. K.; Habib, H. A.; Janiak, C. MOFs as Adsorbents for Low Temperature Heating and Cooling Applications. *J. Am. Chem. Soc.* **2009**, *131*, 2776–2777.
- (30) Fröhlich, D.; Henninger, S. K.; Janiak, C. Multicycle Water Vapour Stability of Microporous Breathing MOF Aluminium Isophthalate CAU-10-H. *Dalton Trans.* **2014**, *43*, 15300–15304.
- (31) Canivet, J.; Bonnefoy, J.; Daniel, C.; Legrand, A.; Coasne, B.; Farrusseng, D. Structure-Property Relationships of Water Adsorption in Metal-Organic Frameworks. *New J. Chem.* **2014**, *38*, 3102–3111.
- (32) Jeremias, F.; Fröhlich, D.; Janiak, C.; Henninger, S. K. Advancement of Sorption-Based Heat Transformation by a Metal Coating of Highly-Stable, Hydrophilic Aluminium Fumarate MOF. *RSC Adv.* **2014**, *4*, 24073–24082.
- (33) Cadiau, A.; Lee, J. S.; Borges, D. D.; Fabry, P.; Devic, T.; Wharmby, M. T.; Martineau, C.; Foucher, D.; Taulelle, F.; Jun, C. H.; Hwang, Y. K.; Stock, N.; de Lange, M. F.; Kapteijn, F.; Gascon, J.; Maurin, G.; Chang, J. S.; Serre, C. Design of Hydrophilic Metal Organic Framework Water Adsorbents for Heat Reallocation. *Adv. Mater.* **2015**, *27*, 4775–4780.
- (34) Jeremias, F.; Khutia, A.; Henninger, S. K.; Janiak, C. MIL-100(Al, Fe) as Water Adsorbents for Heat Transformation Purposes-A Promising Application. *J. Mater. Chem.* **2012**, *22*, 10148–10151.
- (35) Khutia, A.; Rammelberg, H. U.; Schmidt, T.; Henninger, S.; Janiak, C. Water Sorption Cycle Measurements on Functionalized MIL-101Cr for Heat Transformation Application. *Chem. Mater.* **2013**, *25*, 790–798.
- (36) Férey, G.; Draznieks, C. M.; Serre, C.; Millange, F.; Dutour, J.; Surlblé, S.; Margiolaki, I. A Chromium Terephthalate-Based Solid with Unusually Large Pore Volumes and Surface Area. *Science* **2005**, *309*, 2040–2042.
- (37) Férey, G.; Serre, C.; Mellot-Draznieks, C. M.; Millange, F.; Surlblé, S.; Dutour, J.; Margiolaki, I. A Hybrid Solid with Giant Pores Prepared by a Combination of Targeted Chemistry, Simulation, and Powder Diffraction. *Angew. Chem., Int. Ed.* **2004**, *43*, 6296–6301.
- (38) Katz, M. J.; Brown, Z. J.; Colón, Y. J.; Siu, P. W.; Scheidt, K. A.; Snurr, R. Q.; Hupp, J. T.; Farha, O. K. A Facile Synthesis of UiO-66, UiO-67 and their Derivatives. *Chem. Commun.* **2013**, *49*, 9449–9451.
- (39) Park, K. S.; Ni, Z.; Côté, A. P.; Choi, J. Y.; Huang, R.; Uribe-Romo, F. J.; Chae, H. K.; O’Keeffe, M.; Yaghi, O. M. Exceptional Chemical and Thermal Stability of Zeolitic Imidazolate Frameworks. *Proc. Natl. Acad. Sci. U. S. A.* **2006**, *103*, 10186–10191.
- (40) Aristov, Y. I. Challenging Offers of Material Science for Adsorption Heat Transformation: A Review. *Appl. Therm. Eng.* **2013**, *50*, 1610–1618.
- (41) Doonan, C. J.; Tranchemontagne, D. J.; Glover, T. G.; Hunt, J. R.; Yaghi, O. M. Exceptional Ammonia Uptake by a Covalent Organic Framework. *Nat. Chem.* **2010**, *2*, 235–238.